

Suzaku Monitoring of the Seyfert 1 Galaxy NGC5548: Warm Absorber Location and its Implication for Cosmic Feedback

Krongold, Y.¹; Elvis, M.²; Andrade-Velazquez, M.¹; Nicastro, F.^{2,3,4}; Mathur, S.⁵; Reeves, J.N.⁶; Brickhouse, N.S.²; Binette, L.¹; Jimenez-Bailon, E.¹; Grupe, D.⁷; Liu, Y.²; McHardy, I.M.⁸; Minezaki, T.⁹; Yoshii, Y.⁹; and Wilkes, B.²

ABSTRACT

We present a two month Suzaku X-ray monitoring of the Seyfert 1 galaxy NGC 5548. The campaign consists of 7 observations (with exposure time ~ 30 ks each), separated by ~ 1 week. This paper focus on the XIS data of NGC 5548. We analyze the response in the opacity of the gas that forms the well known ionized absorber in this source to ionizing flux variations. Despite variations by a factor ~ 4 in the impinging continuum, the soft X-ray spectra of the source show little spectral variations, suggesting no response from the ionized absorber. A detailed time modeling of the spectra confirms the lack of opacity variations for an absorbing component with high ionization ($U_X \approx -0.85$), and high out-flow velocity ($v_{out} \approx 1040 \text{ km s}^{-1}$), as the ionization parameter was found to be consistent with a constant value during the whole campaign. Instead, the models suggest that the ionization parameter of a low ionization ($U_X \approx -2.8$), low velocity ($v_{out} \approx 590 \text{ km s}^{-1}$) absorbing component might be changing linearly with the ionizing flux, as expected for gas in photoionization equilibrium.

¹Instituto de Astronomia, Universidad Nacional Autonoma de Mexico, Apartado Postal 70-264, 04510 Mexico DF, Mexico.

²Harvard-Smithsonian Center for Astrophysics, 60 Garden Street, Cambridge MA 02138, USA.

³Osservatorio Astronomico di Roma, INAF, Italy.

⁴Foundation for Research and Technology - Hellas (FORTH), University of Crete, Greece.

⁵Ohio State University, 140 West 18th Avenue, Columbus, OH 43210, USA.

⁶Astrophysics Group, School of Physical and Geographical Sciences, Keele University, Keele, Staffordshire ST5 8EH, UK

⁷Department of Astronomy and Astrophysics, Pennsylvania State University, 525 Davey Lab, University Park, PA 16802, USA

⁸School of Physics and Astronomy, University of Southampton, Southampton SO17 1BJ, UK

⁹Institute of Astronomy, School of Science, University of Tokyo, Mitaka, Tokyo 181-0015, Japan

However, given the lack of spectral variations among observations, we consider the variations in this component as tentative. Using the lack of variations, we set an upper limit of $n_e < 2.0 \times 10^7 \text{ cm}^{-3}$ for the electron density of the gas forming the high ionization, high velocity component. This implies a large distance from the continuum source ($R > 0.033 \text{ pc}$; $R > 5000 R_S$). If the variations in the low ionization, low velocity component are real, they imply $n_e > 9.8 \times 10^4 \text{ cm}^{-3}$ and $R < 3 \text{ pc}$. We discuss our results in terms of two different scenarios: a large scale outflow originating in the inner parts of the accretion disk, or a thermally driven wind originating much farther out. Given the large distance of the wind, the implied mass outflow rate is also large ($\dot{M}_w > 0.08 \dot{M}_{accr}$) (the mass outflow is dominated by the high ionization component). The associated total kinetic energy deployed by the wind in the host galaxy ($> 1.2 \times 10^{56} \text{ erg}$) can be enough to disrupt the interstellar medium, possibly quenching or regulating large scale star formation. However, the total mass and energy ejected by the wind may still be lower than the one required for cosmic feedback, even when extrapolated to quasar luminosities. Such feedback would require that we are observing the wind before it is fully accelerated.

Subject headings: galaxies: absorption lines – galaxies: Seyferts – galaxies: active – galaxies: X-ray

1. Introduction

AGN winds, manifested as warm or ionized absorbers (hereafter WA) in the X-ray and UV bands, are found in $\sim 50\%$ of both quasars (Piconcelli et al. 2005) and Seyfert galaxies (Crenshaw et al. 2003). Given their high detection rate and the presence of transverse motion (Mathur et al. 1995; Crenshaw et al. 2003, Arav 2004), it is likely that these systems are present in all AGN, but become visible only when our line of sight crosses the absorbing material. Thus, it has become clear that understanding these winds is crucial to understand the structure and geometry of the nuclear region of quasars (Elvis 2000). Theoretical studies have shown that AGN winds can have an important contribution to cosmic feedback if they carry enough mass and kinetic energy (e.g. Hopkins et al. 2005; Scannapieco & Oh 2004; King 2003).

Despite their relevance, little is known with confidence about the origin, geometry, and structure of AGN winds. However, many physical properties of the absorbing gas are now relatively well understood, as X-ray WAs can be well-described by a few absorbing components in pressure balance, with similar kinematics (e.g. NGC 3783 Krongold et al.

2003, Netzer et al. 2003; NGC985, Krongold et al. 2005a, 2009; Mrk 279 Fields et al. 2007, though see Costantini et al. 2007). This has led to the idea that these winds form a multi-phase medium. The most important remaining unknown of these systems is the location, as their geometry, structure, and cosmic impact all depend critically on their distance to the ionizing source.

Determining the location of the winds is not trivial due to the intrinsic degeneracy of the electron density (n_e) and the distance to the central engine (R) in the equation that defines the two observables: the ionization parameter of the gas ($U_x = Q_x/[4\pi R^2 c n_e]$) and the luminosity of ionizing photons (Q_x). One possible solution to this problem comes from time evolving photoionization, since the ionization equilibrium time of the gas (t_{eq} , i.e. the timescale that the gas requires to reach equilibrium with the ionizing source) explicitly depends on its density (n_e) (e.g. Nicastro et al. 1999; Krongold et al. 2007; among others). By monitoring the response of the gas opacity to ionizing flux variations it is possible to determine n_e and, thus, the location of the WA winds (see Krongold et al. 2007 for further details). Another solution to the above degeneracy relies on measuring line ratios between metastable and stable levels of ions (for instance Li-like ions), which are also sensitive to the electron density (e.g. Gabel et al. 2005). Recently, Rozanska et al. (2008) developed a new technique to estimate the electron density when the dominant heating mechanism of the absorbing gas is free-free absorption by soft X-ray accretion disk photons.

Using these techniques, AGN absorbing winds have been found at distances that range from few light days (Krongold et al. 2007) to hundreds of pc away from the central black hole (Crenshaw et al. 2003). Thus, several locations have been proposed for the origin of the wind including the accretion disk (Elvis et al. 2000), the “obscuring torus” (Krolik & Kriss 2001), and the narrow emission line region (e.g. Kinkhabwala et al. 2002; Ogle et al. 2004). Based on the UV spectra of NGC 3783, Gabel et al. (2005) find a location at ~ 25 pc. for the highest velocity component of the absorber in NGC 3783, and concluded that the gas producing the other two velocity components should lie within that radius. Using X-ray spectra, Netzer et al. (2003) and Behar et al. (2003) placed the absorber in this source at distances larger than 1-3 pc. Krongold et al. (2005b) reported variations in the opacity of the gas in this source and set an upper limit of 6 pc. Reeves et al. (2004) found variability of the Fe XXV and XXVI absorption lines of the high velocity component, and located this hot component within 0.1 pc of the central engine. Kaastra et al. (2004) reported a possible detection of an O V metastable line in the X-ray spectra of Mrk 279, placing the gas at distances of lt-weeks to lt-months of the continuum source. Turner et al. (2008) reported the presence of a partial covering absorber in NGC 3516, and associated this wind with the accretion disk.

Recently, Krongold et al. (2007, hereafter K07) measured short timescale changes in the opacity of the absorbing gas forming the ionized wind in the rapidly variable NLSy 1 galaxy NGC4051. During the ~ 100 ks *XMM-Newton* observation, the flux level of NGC 4051 varied by a factor ~ 10 allowing for a robust determination of the gas response timescale, and thus its electron density and distance. They found that the gas of the two absorbing components present in the absorber is close to photoionization equilibrium on timescales of a few ks during an ionization episode (i.e. when the source flux brightens). However, for the high ionization component of the absorber, during recombination episodes the gas could not reach photoionization equilibrium on timescales ~ 20 ks (it is expected that t_{eq} during recombination is longer than during ionization periods). This allowed them to set a distance of 0.5-1.0 lt-days for the high ionization component of the absorber, and an upper limit of 3.5 lt-days to the distance of the low ionization one. Given that the location of the absorber was inconsistent with the location of the obscuring torus in this source (located at distances $\gg 12$ lt-days, see K07 for details), and that the absorber was detected on an accretion disk scale (distances of a few thousand gravitational radii for the $\sim 1.9 \times 10^6 M_\odot$ central black hole in NGC 4051, Peterson et al. 2004), they concluded that the origin of the wind should be the accretion disk. With the location at hand, K07 suggested a biconical (funnel shaped) wind possibly connected to the high ionization broad emission line region (i.e. consistent with the structure for quasars suggested by Elvis 2000). The mass outflow rate and kinetic energy of the wind were found to be too weak to have any influence on their large scale environment. However extrapolating the values found for NGC 4051 (on the very low end of black hole mass and luminosity) to powerful quasars, they suggested that cosmic feedback was possible for such extreme objects.

Clearly, in order to understand AGN and quasar winds, as well as their connection to other components of the nuclear environment and their possible cosmic feedback, further location measurements are required, on as many objects as possible. Here we present a Suzaku X-ray monitoring campaign for the Seyfert 1 galaxy NGC 5548, designed to follow WA changes in response to continuum variations. The paper is organized as follows: In §2 we describe the reduction of the data. In §3, we present a search for variability in the spectra of the Suzaku data of NGC 5548. In §4 we present the data analysis. In §5 the response of the gas to the continuum variations is further tested. In §6 we present the physical conditions and constrain the location of the absorber, and in §7 we discuss its possible cosmic implications. Finally, in §8 we present our conclusions.

1.1. The Ionized Absorber in NGC 5548

NGC5548 ($cz = 5149 \pm 7 \text{ km s}^{-1}$; De Vaucouleurs, 1991, based on HI measurements) has a black hole mass of $6.7 \times 10^7 M_\odot$ (Peterson et al. 2004) and an X-ray luminosity of $L_{2-6\text{keV}} = (2.0 - 2.8) \times 10^{43} \text{ erg s}^{-1}$ (Andrade Velazquez et al. 2009, hereafter AV09). NGC 5548 has a well known warm absorber. This WA is composed of two velocity components, each with two absorbing gas phases (AV09). It has been observed for ~ 940 ks with the *Chandra* gratings.

AV09 modeled the first 800 ks *Chandra* data of NGC 5548, consisting of ~ 240 ks obtained with the HETG and ~ 560 ks with the LETG (see their Table 1)¹. AV09 resolved two velocity systems in the *Chandra* spectra (as did Steenbrugge et al. 2005) which turn out to correspond to two out of the five CIV absorbing systems observed in the UV (Crenshaw et al. 2009). Each X-ray velocity system consisted of two absorbing components. The high velocity (HV) one (-1040 km s^{-1}) consists of a super high ionization component (or phase, hereafter HV-SHIP), with temperature of $(3 \pm 0.7) \times 10^6 \text{ K}$ ($\log U_x = -1.02 \pm 0.05$) and a high ionization phase (hereafter HV-HIP) with temperature of $(7.8 \pm 1.1) \times 10^5 \text{ K}$ ($\log U_x = -1.58 \pm 0.09$). The high-velocity, super high-ionization component produces absorption from charge states FeXXIII-XXIV, NeX, and, OVIII while the high-velocity, high-ionization component produces absorption by MgXI, and OVIII. The low-velocity (LV) system (-570 km s^{-1}) has one high ionization phase (LV-HIP) with temperature of $(7.8 \pm 1.1) \times 10^5 \text{ K}$ ($\log U_x = -1.58 \pm 0.02$), producing absorption by NeX, MgXII, OVIII; and a low ionization phase (LV-LIP) with temperature of $(3.5 \pm 0.15) \times 10^4 \text{ K}$ ($\log U_x = -2.74 \pm 0.09$) and producing absorption by OVII, OVI, and the Fe M-shell UTA (AV09).

The warm absorber in this source is one of the few where a model consisting of a few components in pressure balance was originally disfavored (Steenbrugge et al. 2005), probably because the two velocity systems were fit together. However, AV09 has shown that, when the absorbers of each velocity component are modeled independently, the WA absorber can be well described by two velocity systems, each consisting of a two phase medium in pressure balance (for a detailed analysis of the WA in NGC 5548 see AV09). A few component, pressure balance model, thus seems generally applicable to WAs.

¹The remaining ~ 137 ks (not modelled by AV09) were obtained ~ 10 days apart from our Suzaku campaign, but the data were acquired during a “low flux state” of NGC 5548 resulting in spectra of very poor S/N.

2. Observations and Data Reduction

NGC 5548 was observed by Suzaku (Mitsuda et al. 2007), as part of a ~ 2 month monitoring campaign. In this work we focus on the XIS data of NGC 5548. The study of the Fe K_α line will be presented in a forthcoming paper (Liu et al. 2010). Simultaneous Swift observations will be presented by Grupe et al. (in preparation).

Suzaku observed NGC 5548 seven times between 18 June 2007 and 6 August 2007 at approximately weekly intervals (with the exception of the week of 30 June), with net exposures of typically 25–35 ks per observation. Table 1 presents the log of observations, exposure time, count rate, and S/N ratio of the data. All observations were performed in the on-axis XIS nominal pointing position. Data from the X-ray Imaging Spectrometer (XIS; Koyama et al. 2007) were analyzed using revision 2 of the Suzaku pipeline². Data were excluded within 436 seconds of passage through the South Atlantic Anomaly (SAA) and within Earth elevation angles and Bright Earth angles of $< 5^\circ$ and $< 20^\circ$, respectively. A cut-off rigidity (COR) of 6 GeV was applied, in order to lower the particle background.

XIS data were selected in 3×3 and 5×5 editmodes using grades 0,2,3,4,6, while hot and flickering pixels were removed using the SISCLEAN script. Source spectra were extracted from within circular regions of $2.9'$ diameter, while background spectra were extracted from circles offset from the source and avoiding the chip corners that contain the calibration sources. The response matrix (RMF) and ancillary response (ARF) files were created using the tasks XISRMFGEN and XISSIMARFGEN, respectively, the former accounting for the CCD charge injection and the latter for the hydrocarbon contamination on the optical blocking filter. Spectra from the two front illuminated XIS 0 and XIS 3 chips were combined to create a single source spectrum (hereafter XIS–FI), while data from the back illuminated XIS 1 chip were analyzed separately. Data were included from 0.45–10 keV for the XIS–FI and 0.45–7 keV for the XIS 1 chip, the latter being optimized for the soft X-ray band. The nominal resolution of both detectors is ~ 75 eV at 2 keV. However, the XIS spectra were subsequently binned to a minimum of 25 counts per bin. χ^2 minimization was used for all subsequent spectral fitting. Net count rates for the XIS–FI range from 0.81 counts s^{-1} (lowest) to 3.60 counts s^{-1} (highest), while the background rate was $< 4\%$ of the source rate during all the observations.

²<http://www.astro.isas.ac.jp/suzaku/analysis/>

3. Monitoring the Gas Response to Continuum Variations I: A Search for Spectral Changes

Figure 1 presents the light curve of the seven Suzaku observations of NGC 5548. The source varied by a factor of ~ 4 during the 2 month monitoring, and up to a factor of ~ 2 between the 1 week observations. It is interesting to note also that significant variability is observed within each observation block. Variations up to 30% are detected on typical timescales of ~ 10 hours (the typical exposure times of the observations, see Liu et al. 2010).

In order to look for any possible variations of the ionized absorber to the variations in the impinging radiation, we have overplotted all the Suzaku spectra on the same scale. This approach is extremely useful when trying to find spectral variations driven by opacity variations in the absorbing gas, given that re-scaling the spectra allows to compare directly the transmission of the absorbing gas from different epochs. We note, however, that the scaling is inappropriate for comparing emission lines since the flux in these features needs to have the continuum subtracted from it. We have chosen Observation 3 (Table 1) as the “standard” normalization point for all observations. Figure 2 presents the normalized spectra for the seven Suzaku observations, along with the normalization factors used to re-scale the spectra. Any variations in the opacity of the gas should be reflected in the soft X-ray band, especially in the range between 0.6 and 1.6 keV (8 and 20 Å), where the majority of the bound-bound and bound-free transitions from the most abundant metals are located. A striking result is that all the seven spectra are extremely similar in this region, indicating that only small spectral variations are present. This lack of variation is further evidenced in Figure 3, where the ratios between the normalized spectra and the spectrum of Observation 3 are presented. In the soft band, the only regions where some variations are observed in all spectra are between 0.5 and 0.6 keV (20 and 24 Å). However, in this region there are not many absorption lines (the strongest are O VII 21.6 Å, and O VI 22.03 Å). Instead, it is likely that such variations are artificially produced by the re-scaling of the spectra, as the O VII emission triplet lies in this region. Some other small variations are present in the soft region on single observations. For instance Observation 6 presents marginal variability near 0.7 and 0.4 keV. Even if such variations are real, they are too small to consider that the gas can reach photoionization equilibrium with the ionizing continuum (as we show below). In the hard region of the spectra, systematic variations are observed with respect to Observation 3, indicating a correlation between the flux level and the X-ray spectral energy distribution of the source (Nicastro et al. 2000; Grupe et al. in preparation).

In Figure 4 the expected spectral variability for an absorber in photoionization equilibrium is presented for a change by a factor ~ 4 in the continuum. To produce this plot, we

have used our best-fit model to the data (presented in §4), with the parameters reported for the Suzaku data in Table 2. From this plot it is clear that, even if small spectral changes are present, the gas does not seem to be responding to the flux changes of the source, and thus, it is likely to be out of photoionization equilibrium.

4. Spectral Modeling of the NGC 5548 Suzaku Data.

To further test the state of the absorbing gas, and quantify its physical properties, we have modeled the Suzaku spectra of NGC 5548. The analysis was carried out with the Sherpa (Freeman et al. 2001) package³ of the CIAO software (Fruscione 2002). The code PHASE (Krongold et al. 2003) has been used to model the ionized absorbers present in NGC 5548. We have explored only photoionization equilibrium models, adopting the same SED used by AV09 (their Figure 4, mostly obtained from the NASA Extragalactic Database, NED)⁴. In this paper, we use the ionization parameter defined in the range 0.1-10 keV (U_x , Netzer 1996). this is different from AV09 who uses the ionization parameter defined over the whole Lyman range. Given the SED, this two quantities are easily related: $\log U_x = \log U - 2.25$.

We have assumed solar elemental abundances (Grevesse et al. 1993). In all the models, we have taken into account Galactic absorption by applying a cold absorption component with an equivalent Hydrogen column frozen to the Galactic value ($N_H = 1.6 \times 10^{20} \text{ cm}^{-2}$, Murphy et al. 1996).

Since our goal is to follow the response of the ionized gas present in the spectra of NGC 5548 using low resolution CCD data, we modeled the data in a fashion similar to Krongold et al. (2007). These authors found that when the kinematic properties of ionized absorbers are constrained by high resolution data, the other properties (ionization parameter and column density) can be well modeled at lower CCD X-ray spectral resolution. Thus, we have modeled the Suzaku XIS spectra of NGC 5548, using the kinematic properties of the absorbers found by AV09 in their spectral analysis on the high resolution, high S/N, *Chandra* data.

AV09 found four absorbing components. Two of these show very different ionization parameters, column densities, and outflow velocities, the HV-SHIP and the LV-LIP. The other two have similar ionization parameters and column densities, but different outflow

³<http://cxc.harvard.edu/sherpa/>

⁴During the SUZAKU monitoring NGC 5548 presented strong changes in the SED (see Grupe et al. in preparation). However, the lack of variability in the absorber to the X-ray continuum changes makes it reasonable to consider a constant SED for the analysis.

velocities, the HV-HIP (with velocity similar to the HV-SHIP) and the LV-HIP (with velocity similar to the LV-LIP). The low resolution of the Suzaku data does not allow us to separate these last two components, even if present in the spectra. Thus, to test their presence, we model them together, using a single absorber (we will call this component [HV+LV]-HIP). In our models of the low resolution CCD Suzaku spectra, we have fixed the outflow velocity, and turbulent velocity of the HV-SHIP and LV-LIP to the best fit values obtained by AV09. To account for the absorption by the [HV+LV]-HIP we have used the average outflow velocity of the HV-HIP and LV-LIP systems found by AV09, and a large turbulent velocity (600 km s^{-1} , similar to the separation of the LV and HV systems). The values used for each component are reported in Table 2.

Using these three absorbing components (HV-SHIP, [HV+LV]-HIP, and LV-LIP), we have searched for possible variations in the opacity of the absorbing gas to the impinging continuum variations. We have used the following approach: (a) we have assumed that no changes are present in column densities during the 2 month monitoring campaign. Therefore, we have set free to vary the column density of each absorbing component, but have forced it to have the same best fit value during all 7 observations. (b) we have left the ionization parameter of each absorbing component free to vary among the observations (as opacity variations should be reflected as variations in the ionization parameter).

We fit simultaneously the XIS-FI and the XIS1 spectra of each observation, and to account for any cross-calibration effect between the two detectors, we have constrained the slope of the power law to be the same, but have allowed the continuum normalizations to vary independently. For each observation, we have produced three different models, including a powerlaw attenuated by one, two, and three absorbing components (HV-SHIP, [HV+LV]-HIP, and LV-LIP), to test the presence and significance of each absorber in the Suzaku data. The seven datasets require the presence of two absorbing components, that correspond to the HV-SHIP and the LV-LIP found by AV09. Figure 5 shows, for Observation 3, the residuals to a model including only a power law (Fig. 5a), a powerlaw attenuated by the HV-SHIP (Fig. 5b), and a powerlaw attenuated by the HV-SHIP and the LV-LIP (Fig. 5c). We note, however, that only for Suzaku Observations 3, 5, and 6 (with larger S/N) is the presence of the [HV+LV]-HIP required by the spectra (although, all datasets are consistent with the presence of this component). Though statistically required for the above 3 spectra, this component does not leave strong (significant) residuals with respect to the model with only two absorbing components. This is expected, given that the [HV+LV]-HIP has an average ionization parameter close to that of the HV-SHIP, but nearly an order of magnitude lower column density. Thus, the overall resonant opacity of the absorber between $5\text{-}15\text{\AA}$ (0.8- 2.5 keV) is mainly driven by the HV-SHIP, and the contribution to the absorption by the HV-HIP is difficult to separate from that component (see Figure 6), especially with low resolution

CCD data. On the other hand, the opacity in the region between 15-20Å (0.6-0.8 keV) is dominated by the LV-LIP. This is probably the reason why the [HV+LV]-HIP component is required only in the 3 observations with larger S/N.

We conclude that changes in the ionization parameter of this component (which represents only the “average” ionization parameter between two different velocity components) cannot be constrained with the present campaign. Therefore, we have included this component in our final models of the Suzaku data leaving the ionization parameter and column density fixed to the best fit values obtained by AV09⁵ (for the value of the column density we have used the sum of the HV-HIP and LV-HIP columns, for the ionization parameter, we have used the average; see Table 2). This component will not be further discussed in the rest of the paper.

When modeling WAs with low resolution data, an important point to keep in mind is any possible degeneracy between the continuum and the opacity of the absorber. Such degeneracy may produce incorrect values of the ionization parameter because of a bad representation of the continuum. When monitoring the response of the gas to continuum variations, such degeneracy may produce “artificial changes” in U_x , or may mask real changes. To test this possible degeneracy we have produced confidence regions between the photon index of the powerlaw and U_x (for both the HV-SHIP and the LV-LIP) for the seven Suzaku observations. In Figure 7 we present the contour plot for Observation 3 and the HV-SHIP. It is clear that both the ionization parameter and the photon index can be measured independently from the data. Similar results are found for both the HV-SHIP and the LV-LIP on all observations. A broad band fit over the XIS and HXD data confirms these results (Liu et al. 2010).

Table 3 presents the best fit continuum parameters, as well as the best fit ionization parameters value, of each observation. Table 2 presents the best-fit column density value of the absorbing components. We note that the fitted N_H values for these absorbing components are consistent within the errors with those found for the *Chandra* best fit model by AV09. This indicates the reliability of the Suzaku data to constrain this parameter over the 7 observations. This further indicates no significant change in column density in ~ 7 years of observations. Using the observed velocities (Table 2), this means that, if moving purely radially, the HV and LV systems have moved at least $\sim (1 - 2) \times 10^{15}$ cm away from the central source.

⁵We note, however, that while this component is required to fit Observations 3,5, and 6, letting the parameters of this component vary has no effect on the results reported in this paper.

5. Monitoring the Gas Response to Continuum Variations II: Time Resolved Modeling of the Ionized Absorber

The ionization parameter of the HV-SHIP and LV-LIP are plotted with the flux level as a function of time in Figure 8. The ionization parameter of the HV-SHIP is consistent with being constant during the seven Suzaku observations (Fig. 8b). Clearly, the absorbing gas forming this component is not varying according to the expectations of photoionization equilibrium (compare Fig 8a with 8b). If the gas were close to photoionization equilibrium, the ionization parameter would vary linearly with the flux (as schematically shown by the red circles in Fig. 8), which is not the case.

Possible changes in U_x are found for the LV-LIP component, which appears to be following more closely the changes in the continuum (compare black squares with red circles in Figure 8c). This would indicate that this component is close to photoionization equilibrium (as all the points are consistent with the expected values from photoionization equilibrium within $\sim 2\sigma$, with the exception of Observation 5, where the difference is $\sim 2.5\sigma$). However, those changes are not visible in Figures 2 and 3, especially in the region between 15-20 Å (0.6-0.8 keV), where the Unresolved transition Array (or UTA) Fe M-shell absorption produced by this component lies. Furthermore, the errorbars in U_x for this component are large, making the values for the seven observations consistent with no variation in the ionization parameter within 2-3 σ . Thus, it is not clear if the apparent variations are real, and masked by the non-variability of the HV-SHIP (which has a column density ~ 10 times larger), or if, as for the [HV+LV]-HIP, the data do not allow us to constrain the response of the gas. We conclude that time-resolved observations with high spectral resolution are required to further constrain the behavior of these two absorbing components. Therefore, hereafter we discuss mainly the behavior of the HV-SHIP, with a few references to the LV-LIP.

5.1. Photoionization Equilibrium Timescales

The HV-SHIP did not vary significantly during the two months of observation, despite the factor ~ 4 variations in the flux of the source. Gas in such conditions, usually remains overionized with respect to the continuum source during the “low flux” states, as t_{eq} during ionization phases is always shorter than t_{eq} during recombination phases (§1). This appears to be the case in NGC 5548 where the HV-SHIP ionization parameter is stuck at high values and does not recombine to reach photoionization equilibrium during the “low flux” observations (Observations 1,2, 7). This is further supported by the fact that the ionization parameter of this component is similar to the one found by AV09 from the average 2000-2005 *Chandra* spectra, with an “average flux” ($F_x[0.5-10 \text{ keV}] \sim 0.011 \text{ ph s}^{-1} \text{ cm}^{-2}$) similar

to the “high flux” levels seen with Suzaku (Observations 3, and 5, see Fig. 1)⁶. This further supports the idea that the gas is close to photoionization equilibrium during these “high flux” states, and provides an a-posteriori justification for using photoionization equilibrium models to fit the spectra.

Given that we do not have continuous observations of the source, we cannot determine the exact moment when the continuum decreased to the “low flux” states. For these observations (1,2, and 7), the flux might have decreased just after the observation began, or at any other time after the previous observation ended. Given that the absorbing gas forming the HV-SHIP did not respond to continuum variations, we have to assume the most conservative scenario, which implies that the change in flux took place just before each “low state” observation started. This means that the gas could not reach photoionization equilibrium with the continuum in the ~ 30 ks that each of these observations lasted. Thus we conclude that the equilibrium time of the HV-SHIP gas is $t_{eq}(\text{HV-SHIP}) > 30$ ks. Note that if the flux decrement took place before the starting point of any of these observations, then the equilibration time could be $\gg 30$ ks.

If the LV-LIP is indeed varying as expected in photoionization equilibrium it can adapt to the continuum changes on a timescale smaller than the time separation between consecutive observations. Thus $t_{eq}(\text{LV-LIP}) < 7$ days ($t_{eq}(\text{LV-LIP}) < 0.6 \times 10^6$ s).

6. The Large Scale Ionized Absorber in NGC 5548

6.1. Physical Conditions

The lower limit on the photoionization timescale of the HV-SHIP ($t_{eq} > 30$ ks) can be used to set an upper limit on the electron density of the absorbing gas, as the first is a function of the second (see Nicastro et al 1999 and Krongold et al. 2007 for further details). We have used the approximate relation between t_{eq} and n_e derived by Nicastro et al. (1999; eq. 5) for a 3-ion atom (i.e. an atom distributed mainly among three of its contiguous ion species):

$$t_{eq}^{x^i, x^{i+1}} \sim \left[\frac{1}{\alpha_{rec}(x^i, T_e)_{eq} n_e} \right] \times \left[\frac{1}{[\alpha_{rec}(x^{i-1}, T_e)/\alpha_{rec}(x^i, T_e)]_{eq} + [n_{x^{i+1}}/n_{x^i}]} \right]$$

⁶We note that the ionization parameter of the HV-SHIP appears to deviate from photoionization equilibrium by $\sim 3\sigma$ in the analysis by AV09. However, this effect is likely caused by AV09 modelling the “average” 2000-2005 *Chandra* spectra of NGC5548, that consists of several datasets with different flux levels (see their Figure 1).

where “eq” indicates the equilibrium quantities, and $\alpha_{rec}(x^i, T_e)$ is the radiative recombination coefficient of the ion x^i , for gas with an electron temperature T_e . This is an excellent approximation for O and Ne for the HV-HIP, that has dominant charge states OVIII-OIX, NeX-NeXI, because 96% of the population of these elements is concentrated in these two ions. We used recombination times from Shull & van Steenberg (1982) and the average equilibrium photoionization temperature (see Table 4). We find $n_e(\text{HV-SHIP}) < 2.0 \times 10^7 \text{ cm}^{-3}$ (we note that the electron density can be much lower than this value, given the very conservative limit on the equilibration time). Using T_e and n_e , we find that the gas pressure $P_e(\text{HV-SHIP}) < 5.8 \times 10^{13} \text{ K cm}^{-3}$.

Assuming the changes in the LV-LIP are real implies $n_e(\text{LV-LIP}) > 9.8 \times 10^4 \text{ cm}^{-3}$ and $P_e(\text{LV-LIP}) > 2.1 \times 10^9 \text{ K cm}^{-3}$ ($T_e(\text{LV-LIP}) \sim 2.1 \times 10^4 \text{ K}$).

6.2. Location and Structure of the Wind

Using the average ionization parameter of the HV-SHIP during the observation ($\log U_x = -.83$) and the luminosity of ionizing photons in the 0.1-10 keV range ($Q_x \sim 9.0 \times 10^{51} \text{ ph s}^{-1}$), we can calculate the value of the product ($n_e R^2$): $1.6 \times 10^{41} \text{ cm}^{-1}$ (Table 4). Given the upper limit on the electron density found above, the distance of the wind to the central engine can be derived. We find $R(\text{HV-SHIP}) > 0.033 \text{ pc}$ ($R(\text{HV-SHIP}) > 1.0 \times 10^{17} \text{ cm}$). Given the black hole mass of NGC 5548 ($M_{BH} = 6.7 \times 10^7 M_\odot$, Peterson et al. 2004), this implies a location in Schwarzschild radii $R(\text{HV-SHIP}) > 5.1 \times 10^3 R_s$.

Assuming a homogeneous flow, and using the column and number densities it is possible to set constraints on the structure of the ionized absorber. The line-of-sight thickness can be estimated as $\Delta R \sim N_H/n_H \simeq 1.23 N_H/n_e$ (where in the last term of the equation we used $n_e \simeq 1.23 n_H$ which is valid for a fully ionized gas with solar abundances), and the relative thickness as $\Delta R/R = 1.23 N_H/n_e R = 1.23 N_H (n_e R^2)^{-1/2} (n_e)^{-1/2}$. We find $\Delta R(\text{HV-SHIP}) > 6.1 \times 10^{14} \text{ cm}$, and $(\Delta R/R)(\text{HV-SHIP}) > 0.007$ (Table 4).

Detmers et al. (2008) found an upper limit of 7 pc for the distance of the absorber producing the O VIII lines, using long term variations (in timescales of years) of the source (though the UV absorbers may be much farther out, i.e. Crenshaw et al. 2009). The HV-SHIP (given its large column density) has the dominant contribution to the absorption by this ion. Locating the absorber at this upper limit of 7 pc would produce a flow with a $(\Delta R/R) < 1.5$. Thus, for this component $0.033 \text{ pc} < R(\text{HV-SHIP}) < 7.0 \text{ pc}$, and $0.007 < (\Delta R/R)(\text{HV-SHIP}) < 1.5$.

For the LV-LIP we find $R(\text{LV-LIP}) < 3.0 \text{ pc}$ ($R(\text{LV-LIP}) < 10^{19} \text{ cm}$, $R(\text{LV-LIP}) < 4.5 \times$

$10^5 R_s$), $\Delta R(\text{LV-LIP}) < 1.3 \times 10^{16}$ cm, and $(\Delta R/R)(\text{LV-LIP}) < 7.6 \times 10^{-4}$, if the putative variations in the opacity of this component are considered as real. Such location is consistent with the upper limits set for this component by Detmers et al. (2008, $R(\text{LV-LIP}) < 19.0$ pc) and Crenshaw et al. (2009, $R(\text{LV-LIP}) < 7.0$ pc).

6.3. Possible Origin and Geometry of the Ionized Outflow

Our results do not allow us to constrain in detail the geometry of the wind. However, the small values of $\Delta R/R$ suggest a compact absorber, and thus it is likely that the structure of the absorber is that of a continuous flow, seen in a transverse direction (Elvis 2000, Arav 2004, K07). The presence of two velocity absorbing systems, each forming a multi-phase wind (AV09), further suggests a transverse outflow. This configuration is consistent with a large scale outflow wind, producing both the absorbing gas, and the extended pc-kpc emitting bicones often found in Seyfert 2 galaxies (Kinkhabwala et al 2002, Sako et al. 2000), as has been explained by K07.

The location and geometry for the ionized absorber in NGC 5548 can be interpreted in terms of two different scenarios: an outflow arising from the innermost regions of the AGN, or an outflow originating much farther out.

6.3.1. An Inner Accretion Disk Outflow

In terms of gravitational radii, the HV-SHIP in NGC5548 can be located at a similar distance (at $> 5000 R_s$) than, for instance, the wind in NGC 4051 (at 2000 to 4500 R_s) which was established to be connected to the inner parts of the accretion disk by Krongold et al. (2007). However, this component could also be located much farther out from the center (given that t_{eq} could be $\gg 30$ ks).

We note that even if this is the case, this does not rule out an origin in the inner accretion disk. If all warm absorbers originate in the inner accretion disk, the fact that different locations have been found (not only between the winds in these two objects, but in many others, see §1) may be simply reflecting that the wind forms in the accretion disk, but extends over a large scale in the nuclear (or maybe even galactic) environment of the active galaxy. We note that a large scale outflow requires that the wind escapes the gravitational well of the central black hole. In order to escape, the wind does not necessarily have to move at escape velocity initially (as stated by several authors), as long as the radiation force on the gas from the continuum source is larger than the gravitational force from the black hole

(see Krongold et al. in preparation). Since both forces depend on the distance as R^{-2} , if radiation pressure dominates at a given distance, it will dominate at any distance, unless the gas opacity changes dramatically, and the gravitational force becomes relatively larger. Thus a large scale outflow is possible even if we do not see the gas moving at escape velocity.

In contrast to NGC 4051, where the absorber’s location was consistent with the Broad Emission Line Region (BELR), in NGC 5548 we are observing the HV-SHIP farther out. The BELR in this object is located at least $\sim 2 - 3$ times closer to the ionizing source (the measured radius is $\sim 0.01 - 0.02$ pc for the H_β line [Bentz et al. 2006] and 0.014 pc for the He II line [Bottorff 2002]). This is consistent with UV observations that suggest that the absorber covers the BELR (Mathur et al. 1995; Crenshaw et al. 2009). In this scenario, any possible connection between the HV-SHIP and the BELR would have to be closer to the accretion disk, at the base of the flow.

The LV-LIP may also be connected to the BELR, since it may be responding in photoionization equilibrium to the changes in the continuum (see §5). In such a case, this velocity component could be located anywhere within 3 pc from the central source, and thus, close the base of the flow. Such a location (~ 0.02 pc) for this component would imply a photoionization equilibrium time scale \sim few minutes.

An intriguing possibility for NGC 5548 is that the two different velocity components found in absorption correspond to two different locations where a single disk wind crosses our line of sight to the central source. This is possible for a bi-conical wind, similar to the one suggested by Elvis (2000) and Krongold et al. (2007). In this case one of the components could be much farther out than the other, which should be close to the base of the wind, near the accretion disk. The relative distance of the two components would then depend on the bending angle of the funnel-shaped wind with respect to the accretion disk, and our line of sight angle with respect to the accretion disk (note that the line of sight angle has to be larger than the wind angle, in order to cross the flow two times). The difference in velocity between the two components does not require strong acceleration for the flow (though this is possible) given that only the radial component of the velocity is measured in the absorbers.

6.3.2. *A Large Scale Origin for the Outflow*

Since ionized absorber winds can arise from both the accretion disk (Everett 2005; Proga 2004) and from the “obscuring torus” (Krolik & Kriss 2001, Dorodnitsyn et al 2008), it is possible that the different locations found for the absorbers may be simply reflecting that we are seeing two different outflows with different origination radius, as suggested by Blustin et

al. (2003). In this case, the different outflow velocity systems found in NGC 5548 may be due to the different locations.

It has been suggested that the “obscuring torus” might be part of an accretion disk wind, whose origin extends from the inner regions of the accretion disk, up to few pc. In such a scenario, a dusty flow is the natural continuation of an inner accretion disk flow beyond the dust sublimation radius (e.g. Elitzur 2008). Whether the obscuring flow is formed by clumps (Nenkova et al. 2008) or not (Chang et al. 2007), it must be neutral close to the disk plane, but could get ionized at larger heights from it. We note that the lower limit on the location of the HV-SHIP is ~ 10 times smaller than the dusty torus location in NGC 5548 (see Fig. 9), that has its hotter parts at $\sim 0.4\text{--}0.45$ pc from the central source, (Suganuma et al. 2006), and it is also below the dust sublimation radius for this object (~ 0.35 pc, based on the UV luminosity of NGC 5548 and the formula given by Barvainis et al. 1987). Thus, the two velocity absorbing systems in NGC 5548 may arise before the dusty wind (in the inner accretion disk as suggested before).

However, just considering the location constraints found here, the origin of both components could be associated with the “extended accretion disk dusty flow”. If ionized absorbers are indeed connected to this outer dusty accretion disk wind, it would be expected that, at least in some of them, a mix of ionized gas and dust is present (given that the dust temperature might be much lower than that of the gas). Indeed, a dusty warm absorber has already been suggested in MCG-6-30-15 (Lee et al. 2001) and IRAS 13349+2438 (Komossa & Breitschwerdt 2000).

Crenshaw, et al. (2009) have shown that the inner nucleus of NGC 5548 is reddened only slightly: $E(B-V) = 0.07$, which corresponds to a column density of $N_H \approx 3.6 \times 10^{20} \text{ cm}^{-2}$ considering a Galactic dust-to-gas ratio. This column density is only a factor ~ 2 smaller than the column density of the LV-LIP. Thus the LV-LIP may contain some dust. This opens the possibility that this component arises in the “extended accretion disk dusty flow”, beyond the dust sublimation radius.

On the other hand, the column density of the HV-SHIP is much larger than the value inferred from the reddening of the inner nucleus, indicating that this absorbing component cannot contain much dust, and therefore is not a dusty outflow. Therefore, if not located before the dust sublimation radius, the most likely location for the HV-SHIP should be much farther out than the “extended accretion disk dusty flow”, and then, (if not arising from the inner parts of the disk) this component should be part of a thermally driven wind (Chelouche 2008).

Clearly, these different scenarios could be easily tested with tighter constraints on the

location of the absorbers.

7. Wind Mass and Kinetic Energy: Implications for Cosmic Feedback

The lower limit on the location of the wind makes possible to estimate a lower limit on the mass and kinetic energy of the flow. We can perform this estimation for a bi-conical wind seen in a transverse direction with respect to our line of sight. For such a geometry Krongold et al. (2007) found that

$$\dot{M}_w = 0.8\pi m_p N_H v_r R f(\delta, \phi)$$

where $f(\delta, \phi)$ is a factor that depends on the particular orientation of the disk and the wind with respect to our line of sight, and for all reasonable angles is of the order of unity (see Krongold et al. 2007, §A.2 for full details). Thus, using the radial velocity, column density, and radius of the HV-SHIP we find that $\dot{M}_w > 0.008 \text{ M}_\odot \text{ yr}^{-1}$. The observed accretion rate in NGC 5548 is $\dot{M}_{accr} = 0.1 \text{ M}_\odot \text{ yr}^{-1}$ (Mathur et al. 1995, assuming a radiation conversion efficiency of 10%), so $\dot{M}_w > 0.08 \dot{M}_{accr}$. We note that this is only a lower limit on the mass outflow rate of the wind, and includes only 1 absorbing component. If this velocity component is indeed composed of a multi-phase medium in pressure balance (AV09), the HV-SHIP and HV-HIP should be co-located. In this case the total mass outflow rate would be $\dot{M}_w > 0.4 \dot{M}_{accr}$. Therefore, the total mass outflow rate of the HV system in NGC 5548 could easily be much larger than the mass accretion rate. We note that a very large rate of mass outflow could present a problem for a radiation driven wind, however, the wind may be magnetocentrifugally launched as suggested by Everett (2005) and then further accelerated by radiation pressure.

We stress here that the implication of large mass outflow rates does not depend on the assumed bi-conical geometrical configuration. If the outflow were considered spherical, then the outflow rate, given by $\dot{M}_w = \Omega m_p n_e R^2 V_r$ (e.g. Steenbrugge et al. 2005), would be nearly two orders of magnitude larger, considering a solid angle of 1.6 sterad (Blustin et al. 2005). A model for the WA in this source, assuming a thermally driven wind arising at $\sim \text{pc}$ from the central engine (Chelouche 2008), also implies a much larger mass outflow rate $\dot{M}_w \sim 0.63 \text{ M}_\odot \text{ yr}^{-1}$. This mass loss rate is similar to the one we would obtain for the HV-SHIP, if this component were located at $\sim 1 \text{ pc}$ from the central engine ($\dot{M}_w \sim 0.25 \text{ M}_\odot \text{ yr}^{-1}$).

Assuming that the black hole mass of NGC 5548 ($M_{BH} = 6.7 \times 10^7 \text{ M}_\odot$, Peterson et al. 2004) was all accreted, and that the ratio $\dot{M}_w / \dot{M}_{accr}$ remained constant, then the integrated lifetime mass lost due to the HV-SHIP X-ray wind would be $M_{out} > 5.4 \times 10^6 \text{ M}_\odot$. Most of the mass would be emitted during the last two doubling times, over outburst lifetimes

estimated to be $\sim 10^7$ yr. This mass, which comes only from one absorbing component, is already similar to the one available from luminous Infrared galaxies (e.g. Veilleux et al. 2005) and, in principle, could all be injected into the interstellar medium of NGC 5548 or the intergalactic medium. This could have important metallicity effects, as it has been shown that the active nuclear environment is enriched in metals, with metallicities a few times solar (e.g. Fields et al. 2005; 2007, Arav et al. 2007) or even larger (Hamman and Ferland 1999).

The total kinetic energy injected by the HV-SHIP in NGC 5548 would be $> 1.2 \times 10^{56}$ erg. Evaporating the ISM from a typical spiral galaxy with galactic disk of radius 10 kpc, disk thickness of 0.1 kpc, and average density of 1 cm^{-3} , requires that this medium be heated to a temperature $T \sim 10^7$ K. The energy needed to increase the ISM of a typical galaxy to this temperature can be estimated as $E \sim N_{tot} kT \sim 10^{57} \text{ erg cm}^{-2} \text{ s}^{-1}$ (where N_{tot} is the total number of particles in the disk). Thus, the kinetic energy injected by the wind can easily supersede the one required to disrupt the interstellar medium. If AGN activity occurs intermittently, then the injected kinetic energy would be lower, and the ISM could have time to fall back. As noted by Krongold et al. (2007), winds moving at $\sim 500 \text{ km s}^{-1}$ can move 5 kpc away in only 10^7 years (compared to the 10^8 yr the AGN estimated lifetime). This implies that AGN warm absorber winds can indeed have important effects on their host galaxies. Among other things, these winds may control or stop large scale star formation processes in their hosts.

If we now assume that the measured ratio $\dot{M}_{out}/\dot{M}_{accr}$ is representative of quasars, then extrapolating these values for wind mass and kinetic energy to powerful quasars ($L_{bol} \sim 10^{47} \text{ ergs s}^{-1}$, $M_{BH} = \text{few} \times 10^9 M_{\odot}$), implies that the total mass injected by these systems in their large scale environment could be $> \text{few} \times 10^8 M_{\odot}$ and the total kinetic energy could be $> \text{few} \times 10^{57} \text{ erg}$. This number is still a small fraction of the 10^{60} erg required by simulations to make quasar winds important for galaxy evolution and IGM structure formation (e.g. Hopkins et al. 2005; Scannapieco 2004; King 2003). However, the above number is only a lower limit, and includes the contribution from only one WA component, with a lower value of the total velocity. In other words, we are taking into account only the radial component of the velocity, and neglecting further acceleration of the flow and mass entrainment.

Recent calculations by Hopkins and Elvis (2009) show that if the AGN wind drives a secondary outflow in the hot, diffuse gas of the ISM, then a mass outflow rate of only $\dot{M}_w \sim 0.05 - 0.10 \dot{M}_{accr}$ for the AGN wind is required for these outflows to have strong evolutionary effects on their hosts. Thus it is possible that WA winds may indeed have a dramatic effect on their large scale environment. Evidently, to further understand the cosmological effects of quasar winds, more theoretical and observational studies are required. As part of an observational program, we are studying the UV and X-ray absorbers on the

Seyfert galaxy NGC 3227.

8. Conclusions

The spectral shape of the soft X-ray spectra of seven Suzaku observations, spanning two months, shows little variation, despite a change in flux by a factor ~ 4 . A detailed modeling of the ionized absorber in this source confirms that the strongest component, the one with the largest velocity and the highest ionization level (HV-SHIP), is not responding as expected in photoionization equilibrium to the impinging continuum. The lack of variation in the opacity of this component implies a density $n_e < 2.0 \times 10^7 \text{ cm}^{-3}$ for the absorbing gas, and a distance $> 0.033 \text{ pc}$ from the central black hole. On the other hand, the ionization state of the absorbing component with low velocity and low ionization (LV-LIP) appears to be varying linearly with the ionizing continuum, suggesting that it is in photoionization equilibrium. In this case, this component should have $n_e > 9.8 \times 10^4 \text{ cm}^{-3}$ and should be located anywhere within 3 pc from the central source.

If the HV-SHIP originates in the inner accretion disk, and we are seeing it farther out, then a large scale outflow may be required. Any relation of this component with the BELR would have to be at the base of the flow, closer in than we are observing it. If the wind starts perpendicular to the disk, and then bends (Elvis 2000), the two absorbing components could be part of the same flow, but at different locations. Alternatively, the HV-SHIP could be arising at a much larger radius, and then it might be a thermally driven wind.

The mass and energy outflow from the wind is dominated by the HV-SHIP. The total kinetic energy ejected by this wind can easily supersede the energy required to disrupt the whole interstellar medium of the host galaxy. This indicates that even winds in Seyferts might have important effects on their hosts, possibly quenching or regulating large scale star formation. However, strong uncertainties in the energetics of these outflows remain. In addition, the total amount of energy required in these outflows for cosmic feedback could be much lower than previously thought (Hopkins and Elvis 2009). Thus, more studies are required to further understand the possible effects of quasar winds on their large scale environment.

This work was supported by the UNAM PAPIIT grant IN118905 and the CONACyT grant J-49594. NSB acknowledges support from NASA to the Chandra X-ray Center through NAS8-03060. This work was supported by NASA grant NNX08AB81G.

REFERENCES

- Arav, N. 2004, ASP Conf. Ser. 311: AGN Physics with the Sloan Digital Sky Survey, 311, 213
- Arav, N., et al. 2007, ApJ, 658, 829
- Andrade-Velazquez et al. 2009, ApJ submitted
- Barvainis R., 1987 ApJ 320, 537
- Behar, E., Rasmussen, A. P., Blustin, A. J., Sako, M., Kahn, S. M., Kaastra, J. S., Branduardi-Raymont, G., & Steenbrugge, K. C. 2003, ApJ, 598, 232
- Bentz, M. C., et al. 2007, ApJ, 662, 205
- Blustin, A. J., et al. 2003, A&A, 403, 481
- Blustin, A. J., Page, M. J., Fuerst, S. V., Branduardi-Raymont, G., & Ashton, C. E. 2005, A&A, 431, 111
- Bottorff, M. C., Baldwin, J. A., Ferland, G. J., Ferguson, J. W., & Korista, K. T. 2002, ApJ, 581, 932
- Chang, P., Quataert, E., & Murray, N. 2007, ApJ, 662, 94
- Chelouche, D. 2008, arXiv:0812.3621
- Crenshaw, D. M., Kraemer, S. B., & George, I. M. 2003, A&A Rev., 41, 117
- Crenshaw, D. M., Kraemer, S. B., Schmitt, H. R., Kaastra, J. S., Arav, N., Gabel, J. R., & Korista, K. T. 2009, arXiv:0902.2310
- Costantini, E., et al. 2007, A&A, 461, 121
- de Vaucouleurs, G. 1991, Science, 254, 1667
- Detmers, R. G., Kaastra, J. S., Costantini, E., McHardy, I. M., & Verbunt, F. 2008, A&A, 488, 67
- Dorodnitsyn, A., Kallman, T., & Proga, D. 2008, ApJ, 687, 97
- Elitzur, M. 2008, New Astronomy Review, 52, 274
- Elvis, M. 2000, ApJ, 545, 63

- Everett, J. E. 2005, *ApJ*, 631, 689
- Fields, D. L., Mathur, S., Pogge, R. W., Nicastro, F., Komossa, S., & Krongold, Y. 2005, *ApJ*, 634, 928
- Fields, D. L., Mathur, S., Krongold, Y., Williams, R., & Nicastro, F. 2007, *ApJ*, 666, 828
- Freeman, P., Doe, S., & Siemiginowska, A. 2001, *Proc. SPIE*, 4477, 76
- Fruscione, A. 2002, *Chandra News*, 9, 20
- Gabel, J. R., et al. 2005, *ApJ*, 631, 741
- Grevesse, M. N., Noels A., & Sauval, A. J. 1993, *A&A*, 271, 587
- Hamann, F., & Ferland, G. 1999, *ARA&A*, 37, 487
- Hopkins, P. F., Hernquist, L., Cox, T. J., Di Matteo, T., Martini, P., Robertson, B., & Springel, V. 2005, *ApJ*, 630, 705
- Hopkins, P. F., & Elvis, M. 2009, arXiv:0904.0649
- Kaastra, J. S., et al. 2004, *A&A*, 428, 57
- Kinkhabwala, A., et al. 2002, *ApJ*, 575, 732
- King, A. 2003, *ApJ*, 596, L27
- Komossa, S., & Breitschwerdt, D. 2000, *Ap&SS*, 272, 299
- Koyama, K., et al. 2007, *PASJ*, 59, 23
- Krolik, J. H. & Kriss, G. A. 2001, *ApJ*, 561, 684
- Krongold, Y., Nicastro, F., Brickhouse, N.S., Elvis, M., Liedahl D.A. & Mathur, S. 2003, *ApJ*, 597, 832 (K03)
- Krongold, Y., Nicastro, F., Elvis, M., Brickhouse, N. S., Mathur, S., & Zezas, A. 2005a, *ApJ*, 620, 165
- Krongold, Y., Nicastro, F., Brickhouse, N. S., Elvis, M., & Mathur, S. 2005b, *ApJ*, 622, 842
- Krongold, Y., Nicastro, F., Elvis, M., Brickhouse, N., Binette, L., Mathur, S., & Jiménez-Bailón, E. 2007, *ApJ*, 659, 1022
- Krongold, Y., et al. 2009, *ApJ*, 690, 773

- Lee, J. C., Ogle, P. M., Canizares, C. R., Marshall, H. L., Schulz, N. S., Morales, R., Fabian, A. C., & Iwasawa, K. 2001, *ApJ*, 554, L13
- Mathur, S., Elvis, M., & Wilkes, B. 1995, *ApJ*, 452, 230
- Mitsuda, K., et al. 2007, *PASJ*, 59, 1
- Murphy, E. M., Lockman, F. J., Laor, A., & Elvis, M. 1996, *ApJS*, 105, 369
- Nenkova, M., Sirocky, M. M., Ivezić, Ž., & Elitzur, M. 2008, *ApJ*, 685, 147
- Netzer, H. 1996, *ApJ*, 473, 781
- Netzer, H., et al. 2003, *ApJ*, 599, 933
- Nicastro, F., Fiore, F., Perola, G. C., & Elvis, M. 1999, *ApJ*, 512, 184
- Nicastro, F., et al. 2000, *ApJ*, 536, 718
- Ogle, P. M., Mason, K. O., Page, M. J., Salvi, N. J., Cordova, F. A., McHardy, I. M., & Priedhorsky, W. C. 2004, *ApJ*, 606, 151
- Peterson B.M. et al. 2004, *ApJ* 613, 682
- Piconcelli, E., Jimenez-Bailón, E., Guainazzi, M., Schartel, N., Rodríguez-Pascual, P. M., & Santos-Lleó, M. 2005, *A&A*, 432, 15
- Proga, D., & Kallman, T. R. 2004, *ApJ*, 616, 688
- Reeves, J. N., Nandra, K., George, I. M., Pounds, K. A., Turner, T. J., & Yaqoob, T. 2004, *ApJ*, 602, 648
- Rózańska, A., Kowalska, I., & Gonçalves, A. C. 2008, *A&A*, 487, 895
- Sako, M., Kahn, S. M., Paerels, F., & Liedahl, D. A. 2000, *ApJ*, 543, L115
- Scannapieco, E., & Oh, S. P. 2004, *ApJ*, 608, 62
- Shull, J. M. & van Steenberg, M. 1982, *ApJS*, 48, 95
- Steenbrugge, K. C., et al. 2005, *A&A*, 434, 569
- Suganuma, M., et al. 2007, *The Central Engine of Active Galactic Nuclei*, 373, 462
- Turner, T. J., Reeves, J. N., Kraemer, S. B., & Miller, L. 2008, *A&A*, 483, 161

Veilleux, S., Cecil, G., & Bland-Hawthorn, J. 2005, *A&A Rev.*, 43, 769

Table 1. Observation summary of the Suzaku XIS monitoring of NGC 5548

Obs. Number	Obs. Id.	Start Time	Exp. Time (ks)	Ct Rate ^a	S/N ^b
Obs 1	702042010	2007-06-18 22:28	31.1	0.81	9.4
Obs 2	702042020	2007-06-24 21:54	35.9	1.42	12.3
Obs 3	702042040	2007-07-08 10:03	30.7	2.97	18.4
Obs 4	702042050	2007-07-15 13:58	30.0	1.83	12.6
Obs 5	702042060	2007-07-22 10:40	28.9	3.60	18.3
Obs 6	702042070	2007-07-29 04:21	31.8	2.36	15.6
Obs 7	702042080	2007-08-05 00:38	38.8	1.23	11.4

^aCount rate in counts s⁻¹ ($0.45 < E < 10.0$ keV). The Ct. Rate corresponds to the XIS–FI chip.

^bSignal to Noise ratio at 15Å (0.83 keV), given for the spectra with nominal binning obtained of the XIS–FI chip.

Table 2. Absorber Parameters

Observation	HV-SHIP ^c			[HV+LV]-HIP ^d			LV-LIP ^c		
	$\log U_X$	$\log N_H^a$	V_{out}^b	$\log U_X$	$\log N_H^a$	V_{out}^b	$\log U_X$	$\log N_H^a$	V_{out}^b
AV09	-1.02 ± 0.05	21.73 ± 0.12	1040 ± 150	-2.74 ± 0.09	20.75 ± 0.3	590 ± 150
HV-HIP (AV09)	-1.58 ± 0.09	21.03 ± 0.07	1180 ± 150
LV-HIP (AV09)	-1.58 ± 0.02	21.26 ± 0.04	400 ± 150
Suzaku ^e	$-0.85^{+0.07}_{-0.08}$	22.0 ± 0.3	1040	-1.58	21.46	790	$-2.78^{+0.27}_{-0.24}$	20.8 ± 0.3	590

^aIn $[\text{cm}^{-2}]$.

^bin km s^{-1} . The outflow velocity was constrained using the best fit values obtained by AV09 over *Chandra* data. The turbulence velocity for the HV-SHIP (160 km s^{-1}) and LV-LIP (100 km s^{-1}) was also constrained using the analysis by AV09. The turbulence velocity of the [HV+LV]-HIP was set to 600 km s^{-1} , the velocity separation between the HV and LV systems.

^cThe column density for the HV-SHIP and LV-LIP was constrained to have a single value for all Suzaku observations.

^dThe column density of the [HV+LV]-HIP from the Suzaku data was fixed to the sum of the columns found by AV09 for the HV-HIP and LV-HIP.

^eThe values for the ionization parameter reported for the Suzaku data correspond to Obs. 3.

Table 3. Continuum, Flux and Ionization Parameter for each Suzaku Observation

Observation	Γ	Norm ^a	$\log U_x(\text{HV-SHIP})$	$\log U_x(\text{LV-LIP})$
Obs 1	1.51 ± 0.02	1.39 ± 0.05	$-0.61^{+0.27}_{-0.09}$	$-3.17^{+0.24}_{-0.25}$
Obs 2	1.59 ± 0.04	2.80 ± 0.08	$-0.87^{+0.13}_{-0.09}$	$-3.98^{+0.39}_{-0.49}$
Obs 3	1.78 ± 0.02	7.96 ± 0.04	$-0.85^{+0.07}_{-0.08}$	$-2.78^{+0.27}_{-0.25}$
Obs 4	1.55 ± 0.01	3.46 ± 0.03	$-0.86^{+0.10}_{-0.09}$	$-3.35^{+0.48}_{-0.18}$
Obs 5	1.69 ± 0.01	7.95 ± 0.04	$-0.86^{+0.07}_{-0.08}$	$-3.30^{+0.10}_{-0.15}$
Obs 6	1.59 ± 0.01	4.66 ± 0.03	$-0.83^{+0.08}_{-0.10}$	$-3.44^{+0.26}_{-0.17}$
Obs 7	1.56 ± 0.01	2.33 ± 0.02	$-0.78^{+0.11}_{-0.13}$	$-3.47^{+0.32}_{-0.19}$

^aAt 1 keV, in units of $10^{-3} \text{ ph cm}^{-2} \text{ s}^{-1} \text{ keV}^{-1}$

Table 4: Physical parameters for the HV-SHIP

N_H 10^{22} cm^{-2}	T_e 10^6 K	$(n_e R^2)$ 10^{41} cm^{-1}	n_e 10^7 cm^{-3}	P_e $10^{13} \text{ K cm}^{-3}$	R 10^{17} cm	ΔR 10^{14} cm	$(\Delta R/R)$
1.0 ± 2.2	2.9 ± 1.4	1.6 ± 0.05	< 2.0	< 5.8	> 1.0	> 6.1	> 0.007

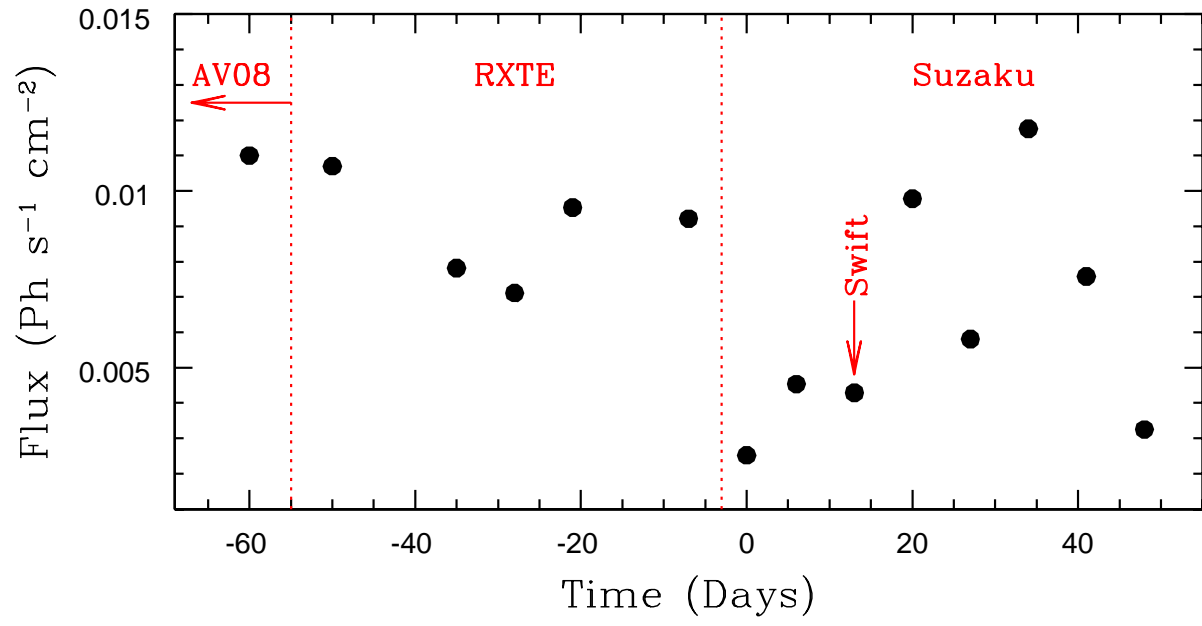


Fig. 1.— 0.5 – 10.0 keV light curve of NGC5548. RXTE and Swift data were taken from Liu et al. (2010) and Grupe et al. (2010).

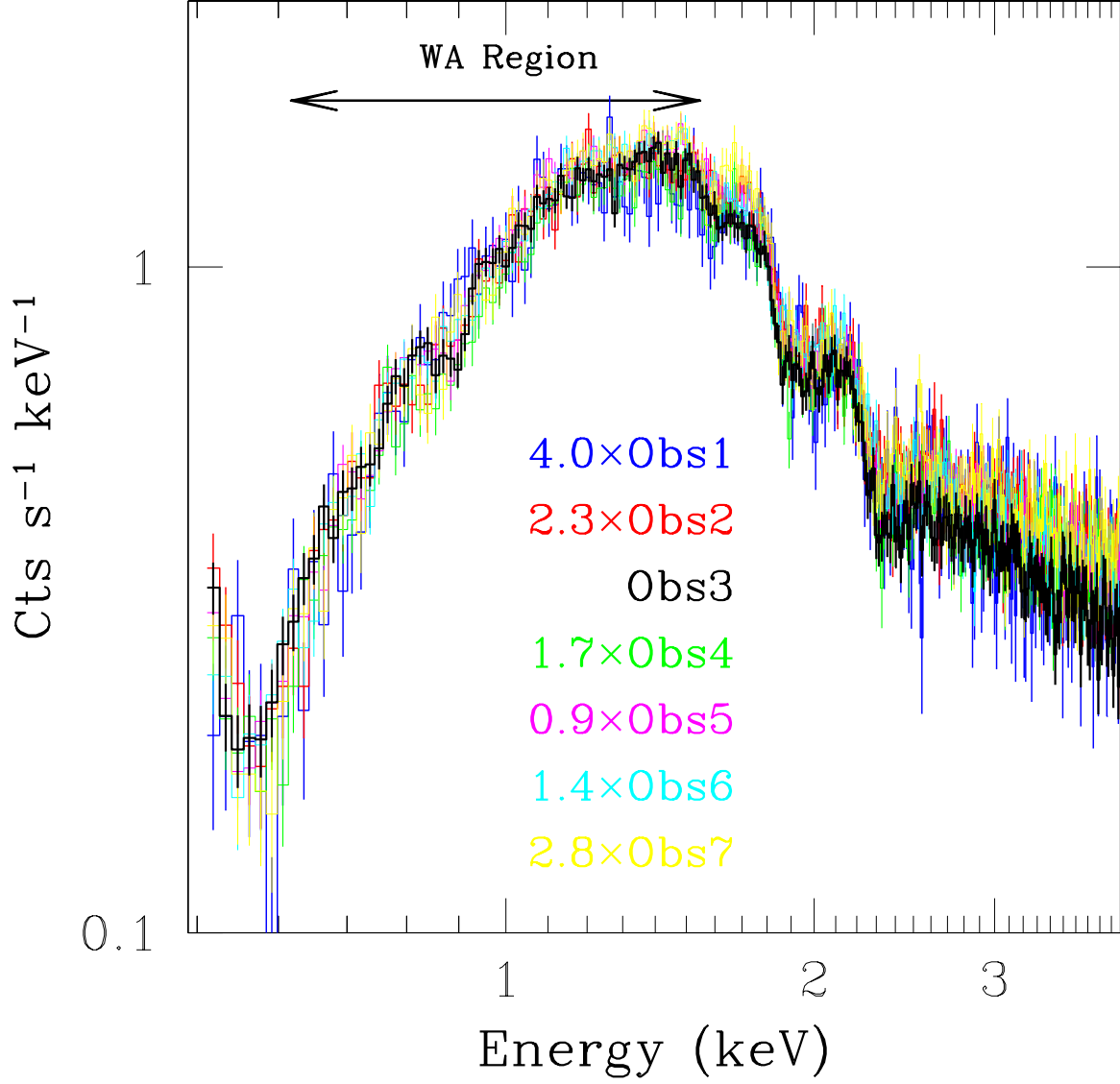


Fig. 2.— XIS-FI Suzaku Spectra of NGC5548. All the spectra are re-scaled with respect to Observation 3, for easy comparison. The data are presented with nominal binning (though the spectral analysis was carried out on data binned including at least 25 cts. per channel). No spectral variations are present between 0.6 and 1.6 keV (8 to 20 Å), indicating no response from the WA to the continuum changes. The changes above 2 keV are due to variations in the X-ray spectral energy distribution of the source (Grupe et al. in preparation).

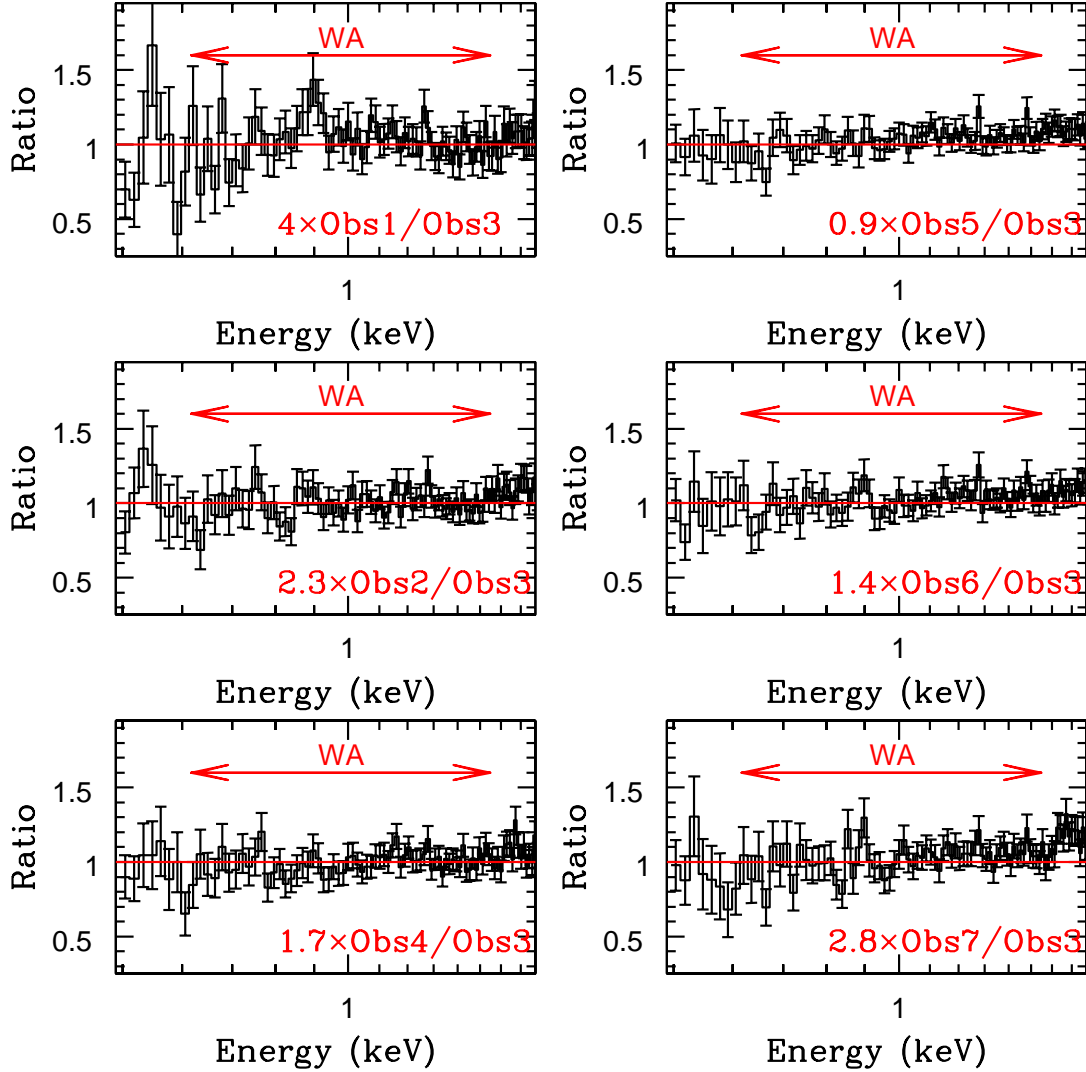


Fig. 3.— Ratio between each XIS-FI observation, and observation 3. The data are presented unbinned (though the spectral analysis was carried out on binned data). In the Warm Absorber region, between 0.6 and 1.6 keV (8 to 20 Å), the ratios are almost flat, confirming the lack of variability in the opacity of the absorbing gas. Changes below 0.6 keV are likely produced by the O VII emission triplet (see text for details).

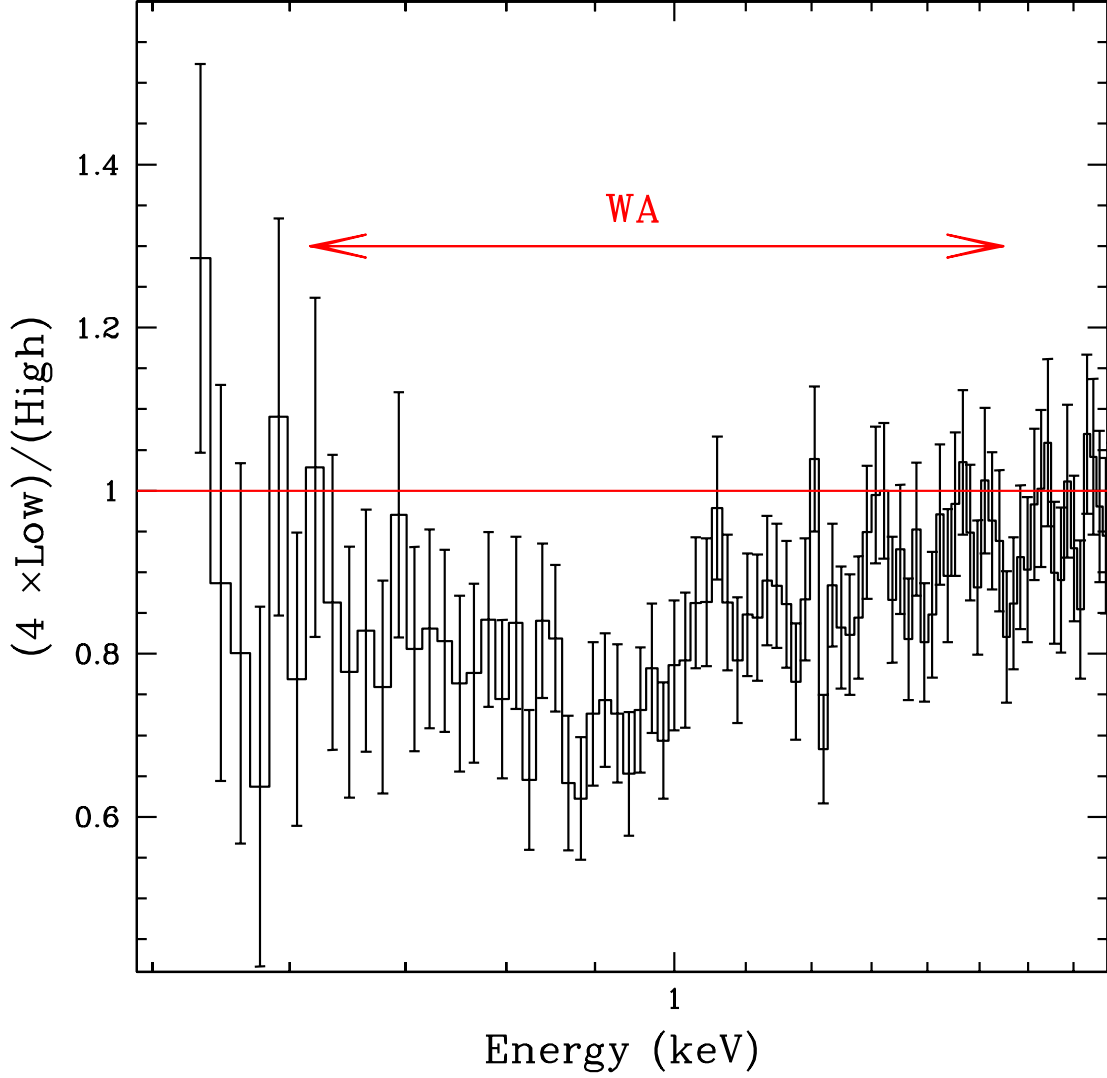


Fig. 4.— Simulated Spectra for the expected spectral variation of an absorber in photoionization equilibrium for a factor ~ 4 in ionizing flux. The exposure times and continuum levels correspond to Suzaku observations 1 and 3. Clearly, such changes would be easily detectable in the data.

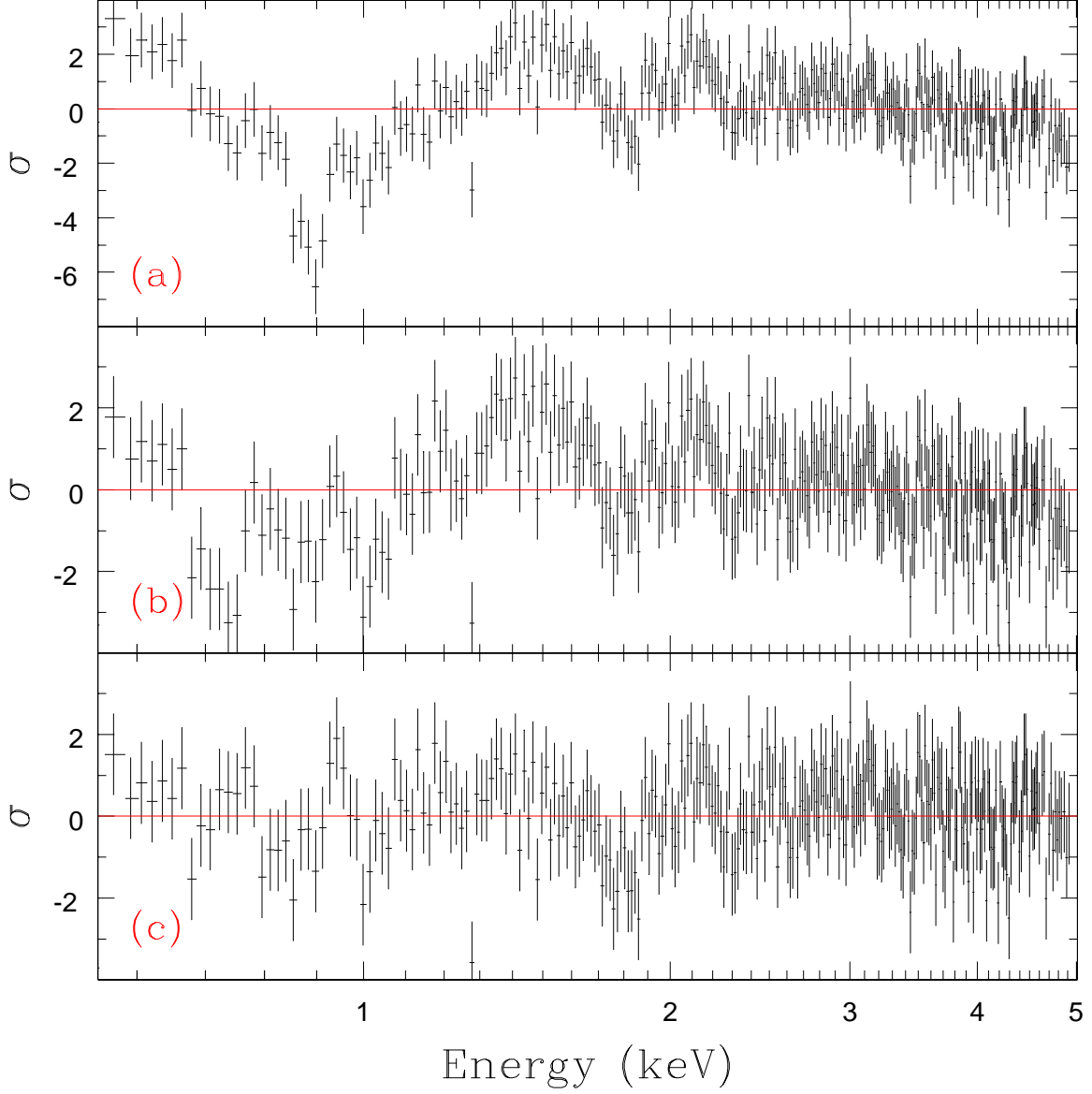


Fig. 5.— Residuals of three different models over Suzaku Obs 3. Panel (a). Residuals to a single powerlaw fit between 2 and 5 keV. The presence of the ionized absorber is evident in the data. Panel (b). Residuals to a fit over the whole spectral range, including a single powerlaw attenuated by one absorbing component. Panel (c). As for panel (b) but including two absorbing components.

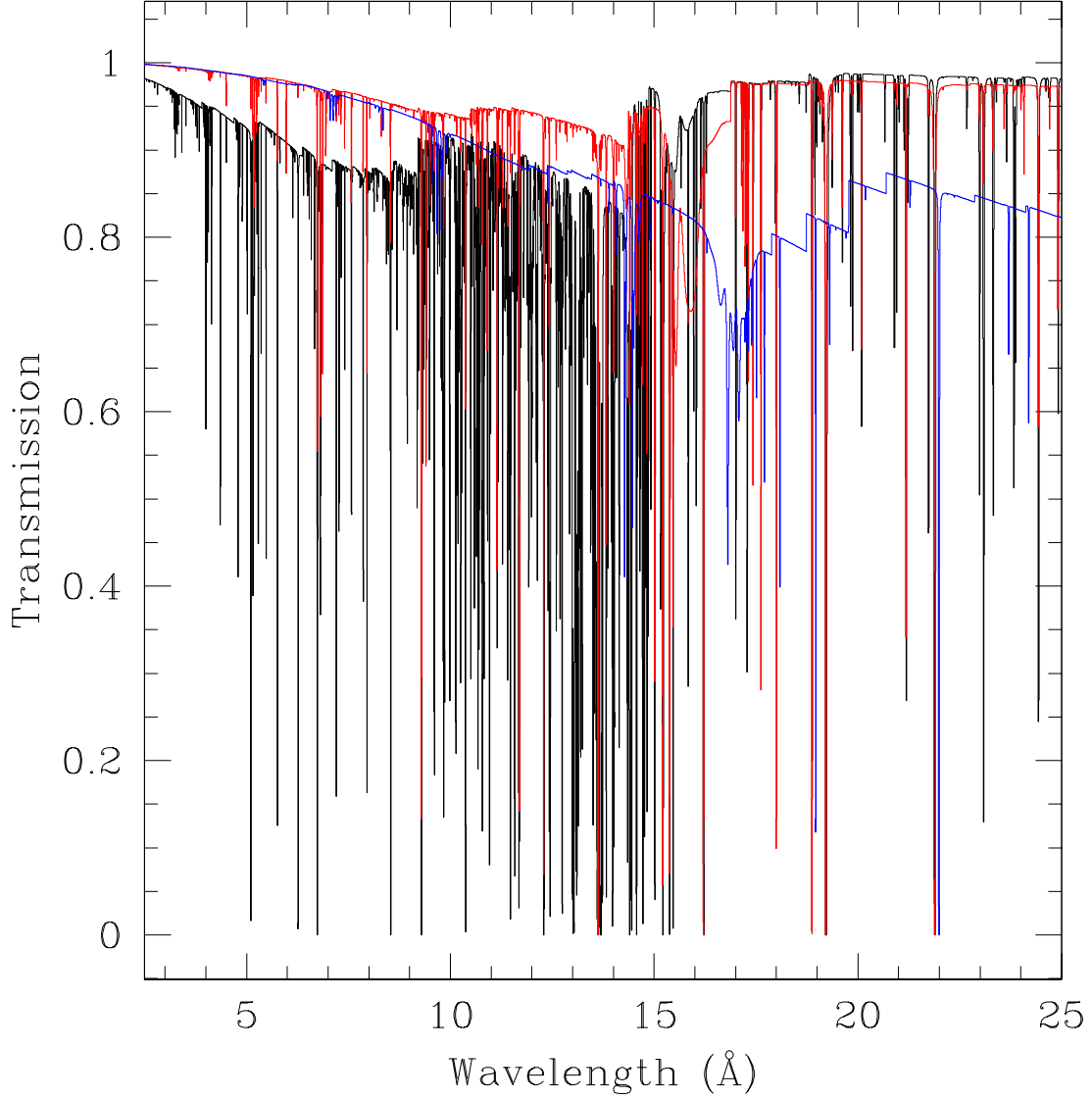


Fig. 6.— Theoretical transmission spectrum of the three absorption components at 0.001 \AA resolution. The HV-SHIP is presented in black, the [HV+LV]-HIP in red, and the LV-LIP in blue. While in the $5\text{--}15 \text{ \AA}$ range most of the opacity is produced by the the HV-SHIP, in the $15\text{--}20 \text{ \AA}$ range the LV-LIP dominates. The different absorption lines blend into broad troughs that allow us to study the WA properties with low resolution CCD data (see Fig. 5).

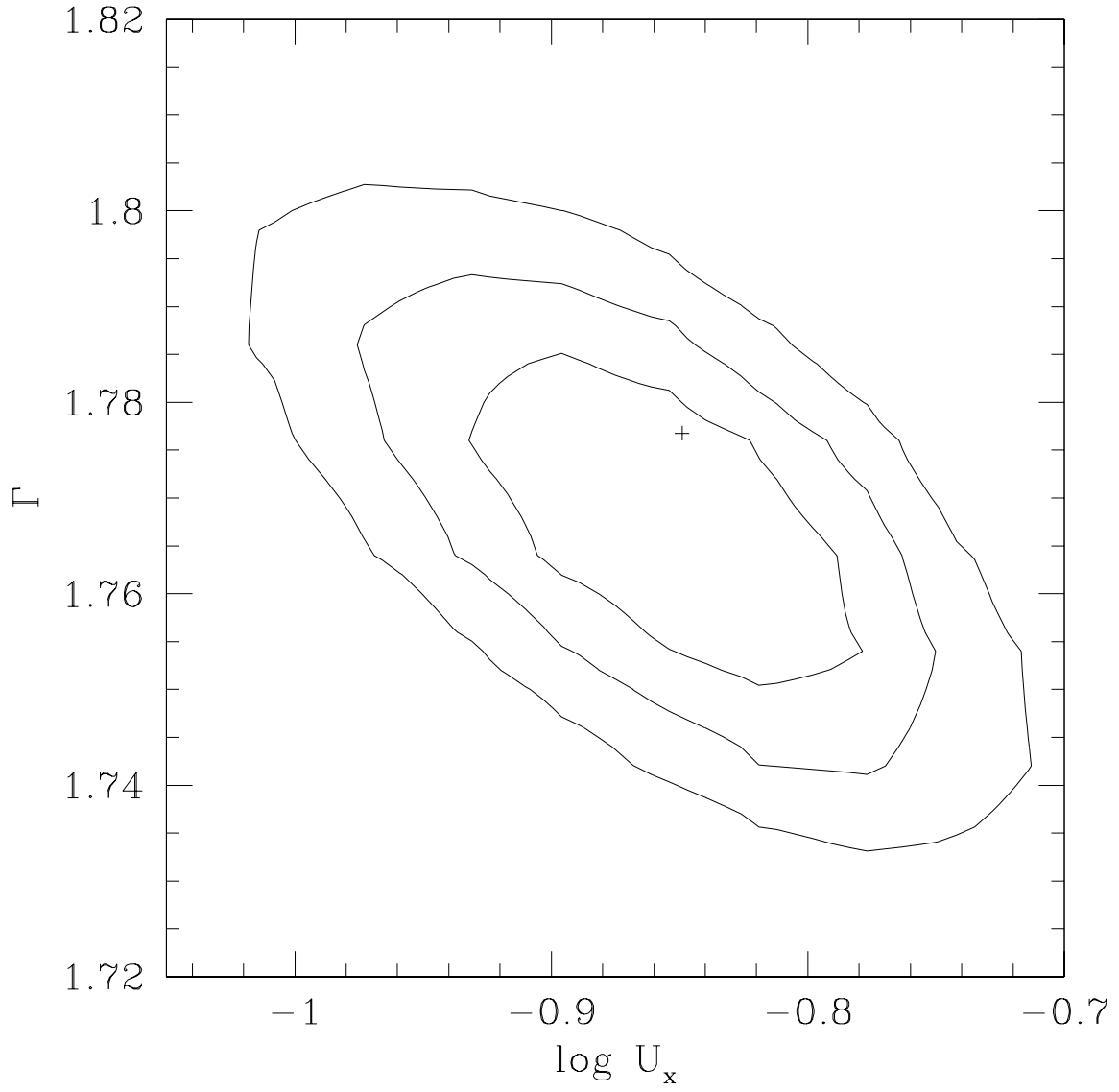


Fig. 7.— Ionization Parameter vs. Photon Index confidence regions (1, 2 and 3 σ) for the fit to Observation 3. Both parameters can be measured independently from the data.

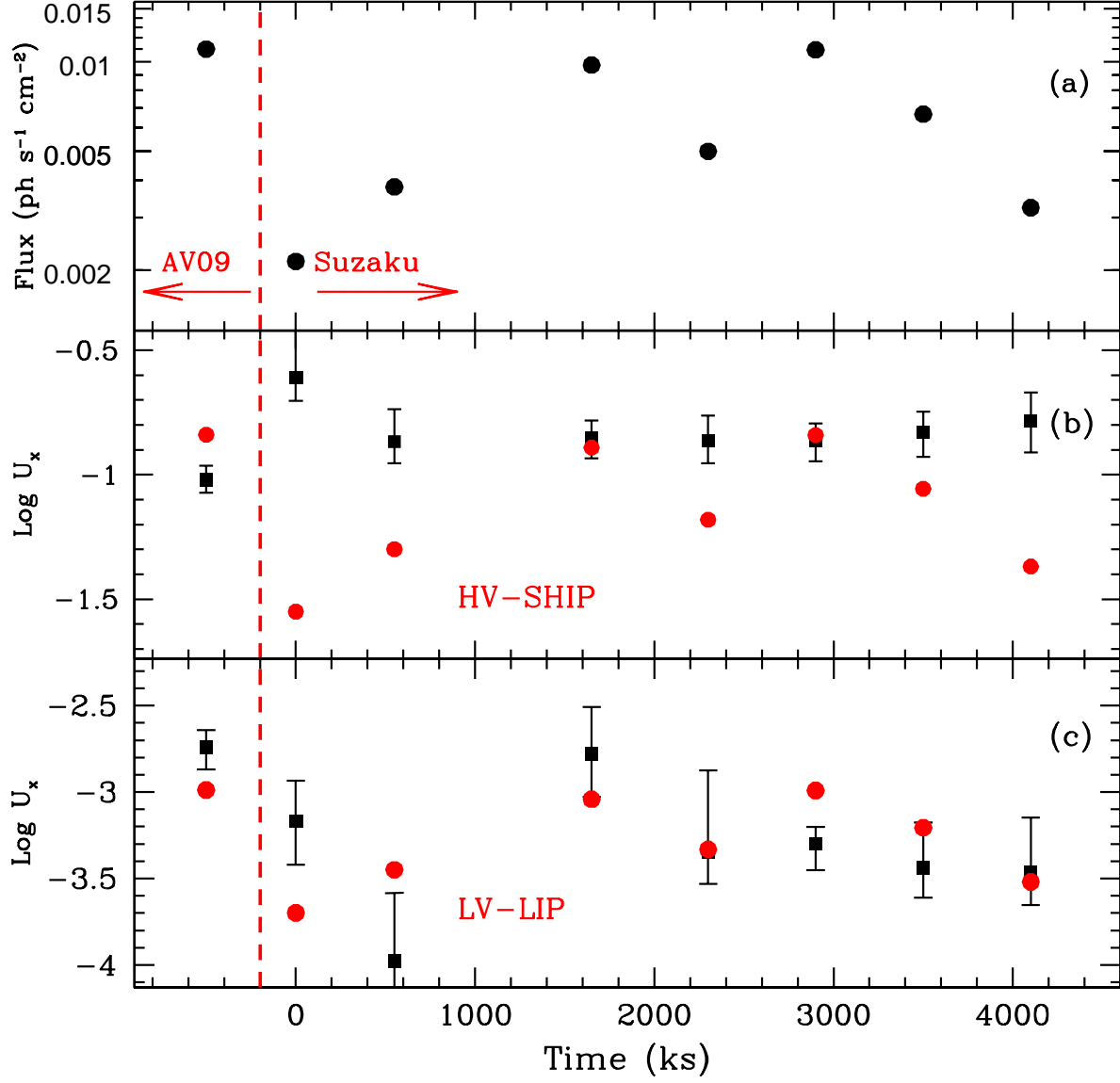


Fig. 8.— Panel (a): Fluxed lightcurve of NGC 5548. The arrows mark the time regions when the object was observed by Suzaku and *Chandra*. Panel (b): Log of the Ionization parameter of the the HV-SHIP vs. time for the 7 Suzaku observations of the source. The analysis on the 2000-2005 *Chandra* data by AV09 is also presented (points with negative time). Panel (c): as panel (b) but for the LV-LIP. The red circles represent expectations for gas in photoionization equilibrium.

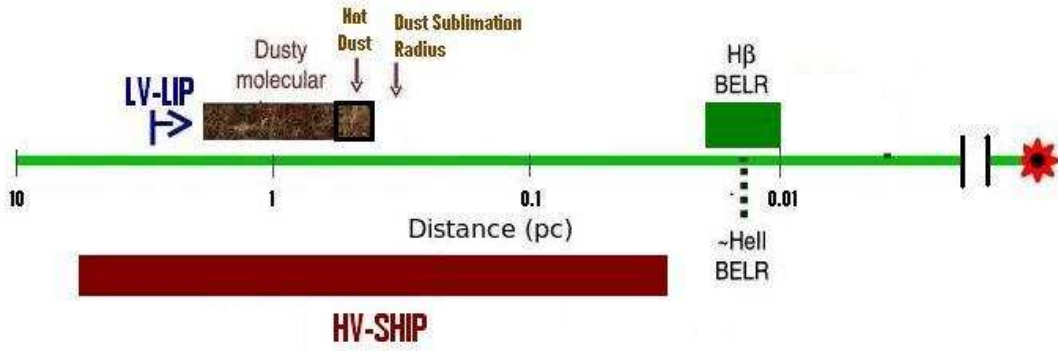


Fig. 9.— Schematic diagram (in logarithmic scale) of the distance to the central source of the different AGN components in NGC 5548